MICROBIOLOGY

Standalone or combinatorial phenylbutyrate therapy shows excellent antiviral activity and mimics CREB3 silencing

Tejabhiram Yadavalli[1], Rahul Suryawanshi[1], Raghuram Koganti[1], James Hopkins[1,2], Joshua Ames[1,2], Lulia Koujah[1,2], Aqsa Iqbal[1], Krishnaraju Madavaraju[1], Alex Agelidis[1], Deepak Shukla[1,2]*

Herpesviruses are ubiquitous human pathogens that tightly regulate many cellular pathways including the unfolded protein response to endoplasmic reticulum (ER) stress. Pharmacological modulation of this pathway results in the inhibition of viral replication. In this study, we tested 4-phenylbutyrate (PBA), a chemical chaperone–based potent alleviator of ER stress, for its effects on herpes simplex virus (HSV) type 1 infection. Through in vitro studies, we observed that application of PBA to HSV-infected cells results in the down-regulation of a proviral, ER-localized host protein CREB3 and a resultant inhibition of viral protein synthesis. PBA treatment caused viral inhibition in cultured human corneas and human skin grafts as well as murine models of ocular and genital HSV infection. Thus, we propose that this drug can provide an alternative to current antivirals to treat both ocular HSV-1 and genital HSV-2 infections and may be a strong candidate for human trials.

INTRODUCTION

The unfolded protein response (UPR) is an important cellular pathway that is initiated as a result of endoplasmic reticulum (ER) stress (*1*–*4*). ER stress is caused by protein accumulation due to excessive misfolded, unfolded proteins in the ER. UPR is the cell's natural response to such events where (i) new protein synthesis is stalled, (ii) protein folding chaperones are up-regulated to ensure timely protein folding, and (iii) misfolded proteins are directed toward degradation (*5*–*8*). Multiple reports in the past have shed light on the cell's UPR pathway to ER stress and have shown that these three legs of UPR when functioning properly can lead to either the alleviation of stress and, hence, survival of the cell or stimulation of apoptosis pathways that lead to cell death (*3*, *9*–*11*). These checks and balances not only ensure healthy maintenance of the cell but also protect a colony of cells from external infections (*1*, *9*, *12*, *13*).

Herpes simplex viruses (HSV-1 and HSV-2) are members of the alpha herpesviruses subfamily and a leading cause of infectious blindness and sexually transmitted disease in the world. While herpes stromal keratitis can result in progressive corneal opacification and vision loss through recurrent HSV-1 infection, HSV-2 infections result in lesions and inflammation around the genital area. In immunocompromised patients and neonates, these viruses can cause systemic infections including but not limited to encephalitis and permanent brain damage. Previous studies have shown that this virus effectively disarms the UPR while extensively producing, folding, and secreting viral proteins from the ER without triggering cell death pathways (*14*–*16*). This robust modulation of UPR by the virus has intrigued the interest of herpesvirologists to uncover underlying mechanisms that can be exploited to control virus replication. An ER-resident prosurvival transcription factor cyclic adenosine 3′,5′-monophosphate (cAMP) response element–binding protein 3 (CREB3) has been in the spotlight as the homolog of HSV-1 VP16, both of which can bind to the host cell factor 1 to initiate transcription of HSV immediate-early genes (*17*). It has also been hypothesized that CREB3 in neuronal cells can facilitate the reactivation of HSV from latency in sensory ganglion cells (*18*, *19*). While the role of CREB3 in the host and during HSV infection has been extensively hypothesized, no evidence currently exists that conclusively details its role in primary infection.

In this study, the modulation of CREB3 by HSV-1 during primary infection using natural target cells was investigated. In addition, the role of CREB3 in HSV-1–induced down-regulation of CCAAT enhancer-binding protein homologous protein (CHOP), an ER stress–dependent apoptosis regulator, was studied. Last, the activity of a chemical chaperone 4-phenylbutyrate (PBA) in alleviating ER stress during HSV infection of the eye, genitals, and brain was assessed. Furthermore, the ocular toxicity profile of a known topical antiviral was determined and observed to be lessened when provided in concert with PBA.

RESULTS

CREB3 is up-regulated upon HSV-1 infection

To understand the behavior of UPR during HSV-1 infection, we performed immunoblotting analysis of common ER-resident regulators ER stress on human corneal epithelial cell line (HCEs). Of all the proteins surveyed, only CREB3 was observed to be up-regulated during infection, while all the other master regulators, such as activating transcription factor 6 (ATF6), phosphorylated protein kinase R-like ER kinase (PERK), phosphorylated eukaryotic translation initiation factor (eIF) 2A, CHOP, calnexin, etc., were mostly down-regulated or remained the same (Fig. 1, A to C). Furthermore, we observed that CREB3 transcription and translation are up-regulated (Fig. 1, D and E) approximately 12 hours postinfection (hpi). In addition, the downstream components of CREB3 (Fig. 1, F and G) such as coatomer subunit beta 1 (COPB1) (*20*) and homocysteine-induced ER protein (Herp) (*21*) were also up-regulated at 24 hpi. However, a differential expression in CREB3-like (CREB3L) proteins was found (fig. S1) with CREB3L1 down-regulated upon infection, while CREB3L2 and CREB3L3 up-regulated. Our results correlate

[1]Department of Ophthalmology and Visual Sciences, University of Illinois at Chicago, Chicago, IL 60612, USA. [2]Department of Microbiology and Immunology, University of Illinois at Chicago, Chicago, IL 60612, USA.
*Corresponding author. Email: dshukla@uic.edu

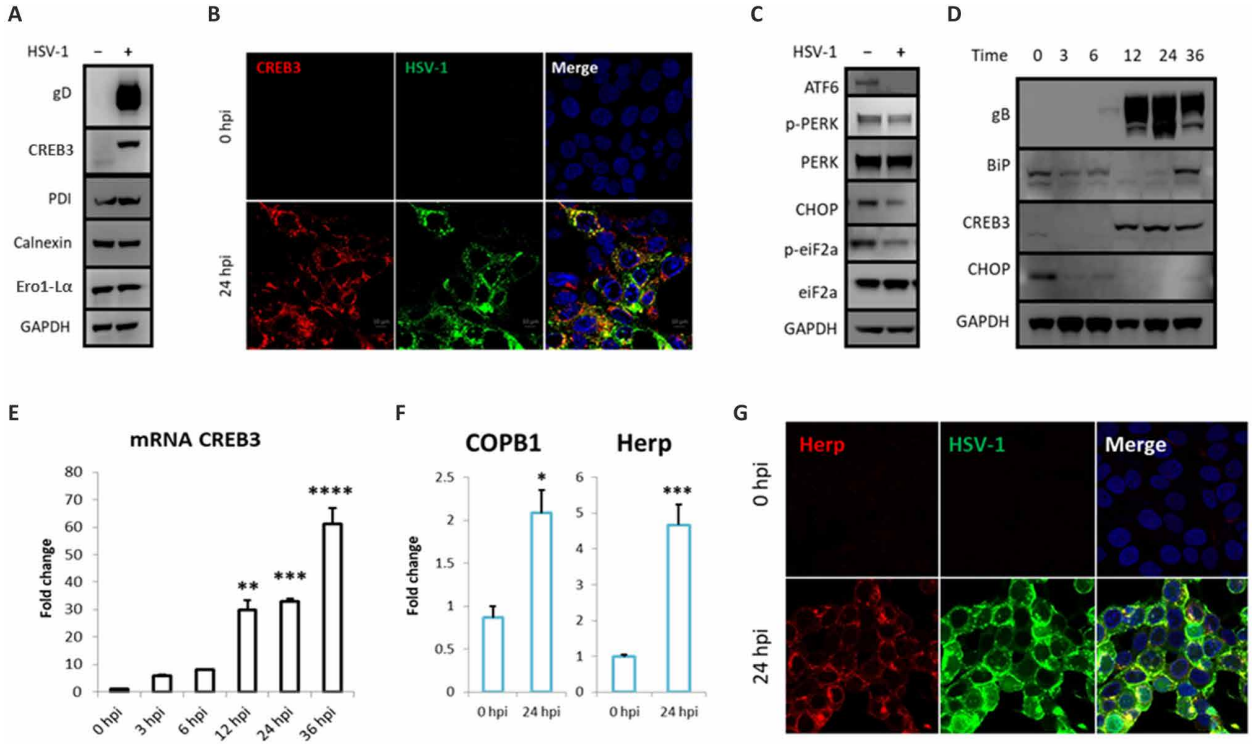

Fig. 1. CREB3 is up-regulated upon HSV-1 infection. HCEs were either mock infected or infected with 0.1 multiplicity of infection (MOI) HSV-1 17 GFP (green fluorescent protein). At 24 hpi, cells were collected and immunoblotted for (**A** and **C**) shown proteins. (**B**) In a similar experiment, cells plated in a glass bottom dish were fixed with 4% paraformaldehyde (PFA) and stained for CREB3 (red), HSV-1 (green), and nucleus (blue). In a time course experiment, HCEs were infected with 0.1 MOI HSV-1 17 GFP for 0, 3, 6, 12, 24, or 48 hours and collected for (**D**) immunoblotting analysis or (**E**) quantitative reverse transcription polymerase chain reaction (qRT-PCR). (**F**) HSV-1–infected HCEs were collected on 24 hpi, and the downstream effectors of CREB3 were analyzed through qRT-PCR and (**G**) fluorescence imaging.

with our observations made in primary HCEs (pHCEs) that were freshly isolated from human donors (fig. S2).

Genetic modulation of CREB3 significantly affects the viral life cycle

Through the observation that HSV-1 infection instigates the up-regulation of CREB3, we hypothesized that the CREB3 might be essential for the positive regulation of viral life cycle. To test this hypothesis, we used a short interfering RNA (siRNA) to inhibit CREB3. Transfecting noninfected cells with this siRNA resulted in a moderate loss of CREB3 protein expression when analyzed through Western blotting analysis (Fig. 2A and fig. S3A). We found that ATF4 and CHOP were mildly up-regulated via CREB3 inhibition (Fig. 2A). Furthermore, when HCEs were transfected with siCREB3 (short interfering CREB3) before infection with HSV-1 17 GFP (green fluorescent protein), we found significant loss of viral spread (Fig. 2B) and viral load when assessed through plaque assay (Fig. 2C) at 24 hpi. Loss of viral spread was also confirmed via flow cytometric analysis (fig. S3B). While silencing of CREB3 resulted in the inhibition of viral replication, we wanted to study whether overexpression of CREB3 was beneficial for viral life cycle. When HCEs were infected with HSV-1 at 0.1 multiplicity of infection (MOI), we did not observe any observable differences in the rate of infection between CREB3-overexpressed and empty vector–transfected control sample. However, there was a significantly higher amount of extracellular secreted virus when analyzed through plaque assay (fig. S4). Another interesting observation was the presence of increased floating dead cells in cell culture in CREB3 down-regulated samples. Given that CREB3 is a known prosurvival factor (*18*, *22*) up-regulated by nuclear factor κB (NFκB) activation (*23*, *24*), we hypothesized that knockdown of CREB3 could result in significant cell death, especially during infection. As suspected, we observed significantly higher cell death in HSV-infected cells that lacked CREB3 when compared with noninfected and nontreated controls (Fig. 2, D and E). On the other hand, we observed a mild (nonsignificant) decrease in cell death upon up-regulation of CREB3 both in noninfected and HSV-1–infected samples (Fig. 2, F and G).

Chemical chaperone PBA treatment mimics CREB3 silencing during HSV-1 infection

After successful genetic modulation, we attempted to understand which pharmacological agent can mirror the CREB3 to uncover potential HSV-1 antivirals. We were looking for agents that were antiviral and did not up-regulate CREB3 but up-regulate CHOP and ATF4 upon their addition. We used various ER stress inducers such as thapsigargin (TG) and tunicamycin (TM) in addition to known ER stress alleviators including salubrinal and PBA for our studies. All drugs except salubrinal showed some degree of antiviral activity (Fig. 3, A and B). Salubrinal showed no antiviral activity on HSV-1–infected HCEs, but on the contrary, HSV-1–infected and salubrinal-treated cells formed large syncytia and survived longer in cell culture than their untreated counterparts (fig. S5). We also found that CREB3 was up-regulated in TG -and TM-treated cells (fig. S6). On the other hand, PBA inhibited HSV-1 infection and did not up-regulate

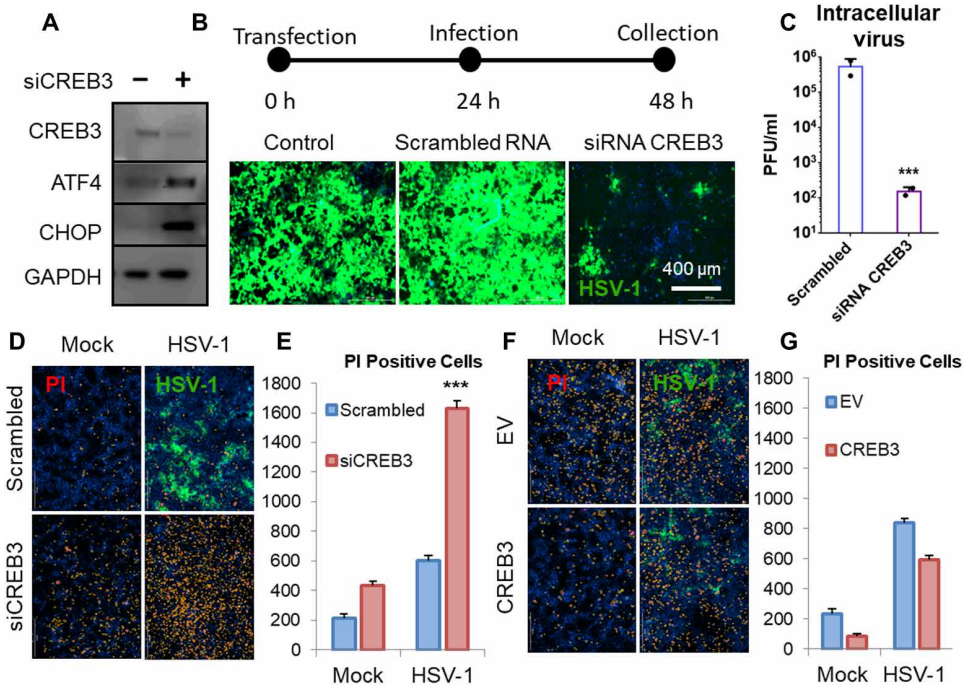

Fig. 2. Modulation of CREB3 expression effects viral life cycle. (**A**) HCEs were transfected with CREB3 siRNA for a period of 24 hours, and the cell lysates were immunoblotted for the shown antibodies. Glyceraldehyde-3-phosphate dehydrogenase (GAPDH) was used as loading control. (**B**) HCEs were transfected with CREB3 siRNA for a period of 24 hours before the addition of 0.1 MOI HSV-1 17 GFP. At 24 hpi, cells were (A) imaged using a fluorescence microscope. (**C**) Cell lysates from the cell culture were used as inoculum for a plaque assay on Vero cells. (**D**) HCEs were transfected with CREB3 siRNA or scrambled siRNA for a period of 24 hours and then infected with mock or HSV-1 17 GFP (green) strain for a period of 24 hours in the presence of propidium iodide (PI) (red) to signify cell death. (**E**) Quantification of the number of cells stained with PI in multiple frames. (**F**) HCEs were transfected with CREB3 plasmid or empty vector pcDNA plasmid for a period of 24 hours and then infected with mock or HSV-1 17 GFP (green) strain for a period of 24 hours in the presence of PI (red) to signify cell death. (**G**) Quantification of the number of cells stained with PI in multiple frames. Nonparametric Student's *t* test was conducted to determine significance. ***$P < 0.001$.

CREB3 but up-regulated CHOP and ATF4 at a concentration of 10 mM (Fig. 3C). Immunoblotting for cytoplasmic and nuclear proteins revealed that PBA-treated samples had increased nuclear presence of ATF4 and CHOP in addition to decreased CREB3 and NFκB translocation to the nucleus (Fig. 3D). We also observed that PBA-treated noninfected cells had greater viability in cell culture compared with infected samples (fig. S7A). Furthermore, no difference in viral entry was observed at viable concentrations of PBA and inhibited virus in a concentration-dependent manner (fig. S7, B and C).

Therapeutic treatment with PBA can be an effective strategy to curb HSV infection ex vivo and in vivo

After characterizing the antiviral potential of PBA in vitro, we proceeded to test whether this chemical chaperone can control HSV-1 replication in human tissue explant models. Our infection studies on donated human corneas revealed that PBA treatment was as effective as acyclovir (ACV) in curbing HSV-1 (Fig. 4, A and B). These results were consistent with experiments conducted on primary HCEs that were isolated from donated human corneas (Fig. 4, C and D). Furthermore, using primary human skin grafts, we observed that PBA treatment was effective in controlling HSV-1 skin infections (Fig. 4E and fig. S8).

Having established the antiviral efficacy of PBA ex vivo, we then investigated the potential therapeutic role of PBA in a murine model of ocular HSV infection. All the experiments were performed using five female mice per group infected in their left eye with 5×10^5 plaque-forming units (PFU) McKrae HSV-1 strain. Treatments were started 1 day postinfection (dpi) and continued until 10 dpi. We administered either PBA (50 mg/kg) or ACV (5 mg/kg) as positive control or equivalent volume of mock phosphate-buffered saline (PBS) as a negative control once every day intraperitoneally. Ocular washes collected on 2 and 4 dpi were used to assess viral shedding through plaque assay (Fig. 5B) and imaged on 7 dpi to record manifestation of the disease. No blepharitis, corneal/stromal keratitis, or ulceration was seen in PBA- and ACV-treated mice; however, PBS-treated mice succumbed to all three (Fig. 5A). Animals were observed until 28 dpi when they were euthanized, and left trigeminal ganglion was collected to check for latency. The trigeminal ganglia collected on 28 dpi also did not show any reactivated virus for PBA- and ACV-treated mice (fig. S9).

In a parallel study, we conducted in vitro antiviral studies against HSV-2 (fig. S10) before naïve BALB/c mice were injected subcutaneously with medroxyprogesterone (2 mg per mice; Depo-Provera) 5 days before intravaginal HSV-2 infection (5×10^5 PFU). Starting 1 dpi, we treated the mice by intraperitoneal injections of ACV and PBA at doses similar to those mentioned above. As expected, we observed no genital ulceration and reduced viral titers in vaginal swabs collected on 2 and 4 dpi (Fig. 5, C and D) for PBA- and ACV-treated mice.

PBA synergizes with known topical antiviral to reduce effective concentration

In our preliminary study to understand the topical antiviral efficacy of PBA, we infected murine corneas with HSV-1 before dosing them

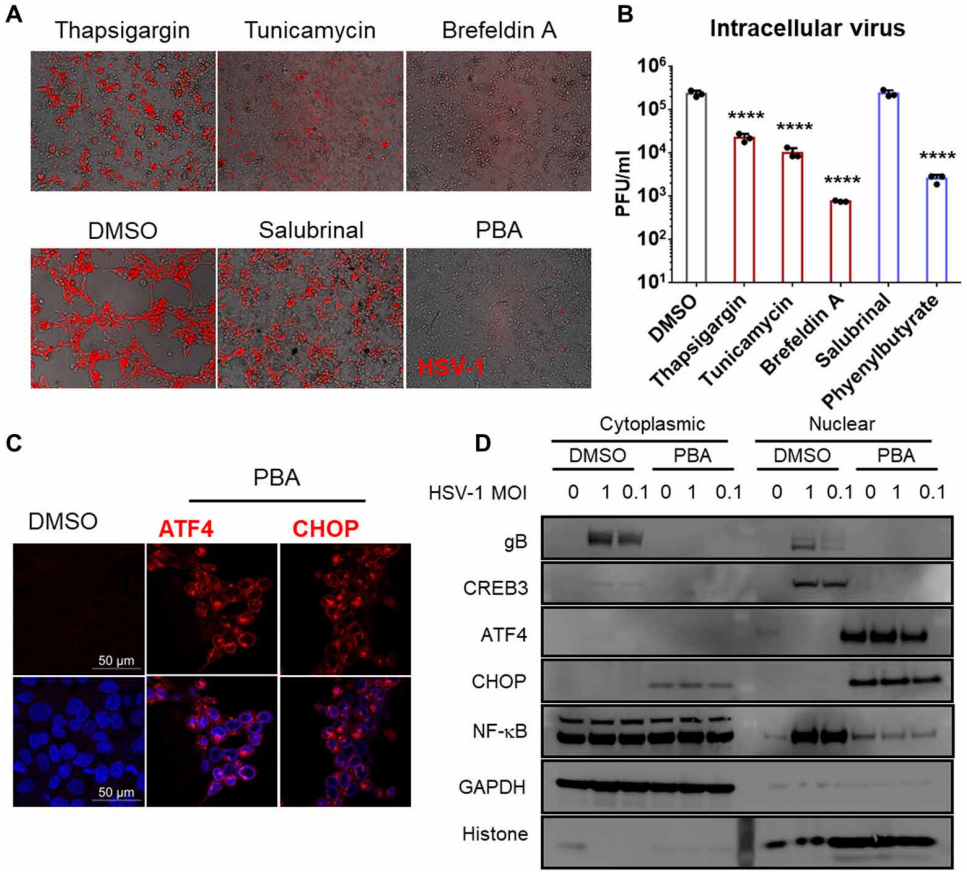

Fig. 3. ER stress alleviation through PBA reduces viral infection and induces CHOP and ATF4 expression. HCEs were infected with 0.1 MOI HSV-1 17 GFP (pseudo-colored red) and treated with tunicamycin (1 μM), thapsigargin (1 μM), brefeldin A (1 μM), salubrinal (75 μM), or PBA (10 mM). At 24 hpi, cells were (**A**) imaged for the presence of fluorescent HSV-1, and (**B**) cells were lysed and used as inoculum on Vero cells to assess viral titer via plaque assay. Multiple Student's *t* test was conducted to determine significant difference between dimethyl sulfoxide (DMSO)–treated and drug-treated samples. ****$P < 0.0001$. (**C**) HCEs plated in glass bottom dishes were treated with mock DMSO or PBA (10 mM) for 24 hours before fixing them with 4% PFA and staining them with fluorescently labeled antibodies. These dishes were imaged at 63× on a Zeiss confocal microscope. (**D**) HCEs were infected at MOI of 0, 1, or 0.1 for 24 hours in the presence or absence of PBA. Cells were lysed in a hypotonic buffer to remove the cytoplasmic protein portion followed by radioimmunoprecipitation assay buffer to extract nuclear proteins. The samples were separated and immunoblotted for shown proteins. GAPDH was used as loading control.

every day three times with PBA, trifluridine (TFT), or PBS control. To our surprise, preliminary studies on PBA did not show any topical antiviral activity at 10 mM concentration, perhaps due to the poor bioavailability on the corneal surface. However, in our in vitro studies, as mentioned previously, PBA showed potent antiviral activity. In this regard, we hypothesized that PBA when synergized with TFT might be able to reduce the effective concentration to inhibit viral replication. As hypothesized, we saw antiviral synergy at concentrations as low as 1.25 mM for PBA and 0.81 μM for TFT when added in tandem, compared with adding those drug concentrations alone (Fig. 6, A and B). This led us to our next experiment to observe whether a synergy between TFT and PBA would work in a murine model of ocular infection. The results from this experiments showed that we can lower the effective antiviral concentration of TFT from 50 μM (administered three times a day) to 25 μM (three times a day) when used in synergy with PBA (5 mM), effectively cutting the requisite concentration in half (Fig. 6, C and D, and fig. S11).

The advantage of this reduction in concentration is that TFT is known to cause ocular irritation when used for a prolonged period of time. Hence, we hypothesized that a synergistic formulation can effectively reduce any toxic symptoms associated with TFT. To test this hypothesis, we performed a 4-week ocular toxicity profile study using PBS (control), PBA (10 mM), TFT (50 μM), and PBA (5 mM) + TFT (25 μM). At the end of this study, the results showed that PBA alone and PBA + TFT showed no increase in surface dryness, corneal inflammation, corneal sensitivity, and ocular hypertension. However, TFT alone at 50 μM concentration caused significant surface dryness and loss of corneal sensitivity at the end of 4 weeks with no changes to corneal thickness and intraocular pressure (fig. S12).

Synergistic PBA formulation can protect from HSV encephalitis

Once we observed the synergistic ability of PBA with TFT, we sought to test whether the same can be applied to other well-known anti-HSV nucleoside analogs. As expected, PBA showed effective anti-HSV synergy with ACV, ganciclovir, pencyclovir, valacyclovir, and famcyclovir, effectively reducing the required concentration by approximately 100-fold in vitro (fig. S13).

We then attempted to replicate this behavior in vivo in a murine model of HSV encephalitis [Fig. 7A; (*25*, *26*)]. Murine model of HSV

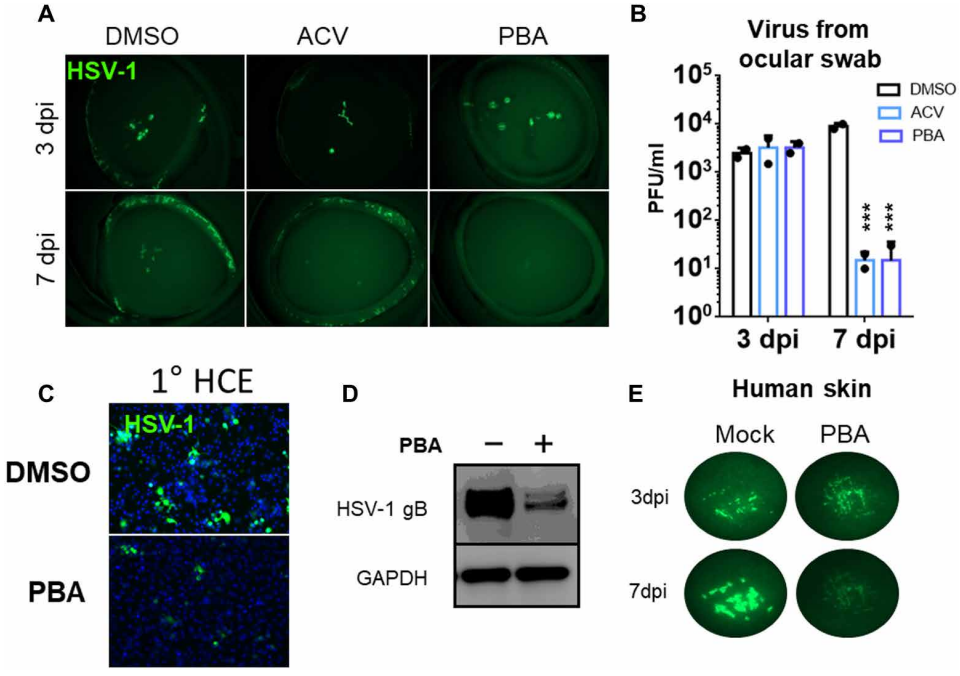

Fig. 4. Therapeutic efficacy of PBA in ex vivo human tissues. Human corneas that were infected with HSV-1 17 GFP for 3 days before ACV (50 μM), PBA (10 mM), or DMSO were added to the cornea culture media. (**A**) Images were procured using a stereoscope on 3 and 7 days postinfection (dpi) to visualize viral spread. (**B**) Swabs taken from the corneal tissue were titrated using plaque assays. (**C**) Primary epithelial cells were isolated from human corneas and infected with HSV-1 17 GFP followed by treatment with PBA (10 mM) or DMSO control. At 24 hpi, images were taken at 10× using a fluorescence microscope. (**D**) Cell lysates were immunoblotted for the presence of viral proteins. (**E**) Human skin samples procured from Genoskin were cultured according to the manufacturer's protocol. Skin epithelium was abraded using a sharp blade and infected with HSV-1 17 GFP. At 3 dpi, fluorescence image of the skin was acquired using a Zeiss stereoscope. PBA was administered to the skin systemically by adding PBA (10 mM) to the growth media provided by the manufacturer. At 7 dpi, fluorescence images were taken again to assess extent of viral spread in the skin samples. Two-way analysis of variance (ANOVA) was used to assess significant differences. ***$P < 0.001$.

encephalitis results in 100% death of BALB/c mice within 10 dpi when infected intranasally with 10^5 PFU McKrae strain of HSV-1 (Fig. 7, B and C). We observed that only ACV (50 mg/kg) administered twice a day intraperitoneally was able to show protective effects including 0% animal death, minor (<10%) weight loss, and no behavioral deficits. However, ACV at 10 mg/kg or PBA at 400 mg/kg only showed partial protection where up to 50% animal death was observed with an average of 20% weight loss and >50% showing behavioral changes (Fig. 7, D and E). In addition, PBA at 100 mg/kg showed no protection at all with 100% animal death with rapid weight loss (>30%) and hunch back, secluded behavior. Meanwhile, infected mice administered with a cocktail of ACV (10 mg/kg) and PBA (100 mg/kg) showed only mild symptoms of disease progression (<10% weight loss) and no behavioral changes and made a complete recovery with no deaths reported in that group at the end of the experiment 10 dpi.

DISCUSSION

Our study demonstrated a strong antiviral activity of PBA against HSV-1 infection. Using several different in vitro, ex vivo, and animal models of infection, we found that PBA was highly effective in reducing HSV infection, and the levels of antiviral activity were similar to a currently prescribed antiviral for human HSV infections. At its therapeutic concentration, we show that PBA regulates ER stress without any adverse toxicity to cells. ER stress is one of the main stress pathways that the virus uses to regulate its replication inside a host cell. It does so by controlling important ER membrane proteins to its own advantage, which regulate the three main branches of UPR (*7*, *12*, *27*). While CREB3's functional role in regulating Golgi and ER stress has been discussed previously, its role during HSV infection has not been systematically studied to the best of our knowledge. Hence, in this study, we focused on how CREB3 expression is modulated during HSV-1 infection. We observed that CREB3 and its downstream elements Herp and COPB1 are up-regulated upon infection. We and other groups have previously shown that NFκB is up-regulated and translocated to the nucleus upon infection (*28*–*31*). CREB3 is one of the many genes that are transcribed by this transcription factor that functions as a prosurvival factor during cellular stress (*10*, *18*, *22*). The up-regulation of CREB3 may be NFκB dependent, although testing that hypothesis is out of the scope of this study. Silencing CREB3 expression resulted in loss of infection, pointing to the possibility that HSV-1 uses CREB3 and its downstream elements to its own advantage during infection. However, increasing extrinsic expression of CREB3 only showed minor increase in viral load, especially in secreted viruses. Furthermore, CREB3 silencing increased CHOP, an ER stress–inducible proapoptotic protein, and had a major impact on the survival of the cells, especially during HSV-1 infection, confirming its role as a prosurvival factor during cellular stress conditions (fig. S17).

Given its antiviral nature, we tried to find a pharmacological mimic to CREB3 silencing. Unlike TM, TG, and salubrinal, PBA not only was able to inhibit viral replication but also did not induce CREB3 expression and increased CHOP and ATF4 in the nucleus (fig. S17). In addition, PBA-treated HSV-1–infected cells did not show translocation

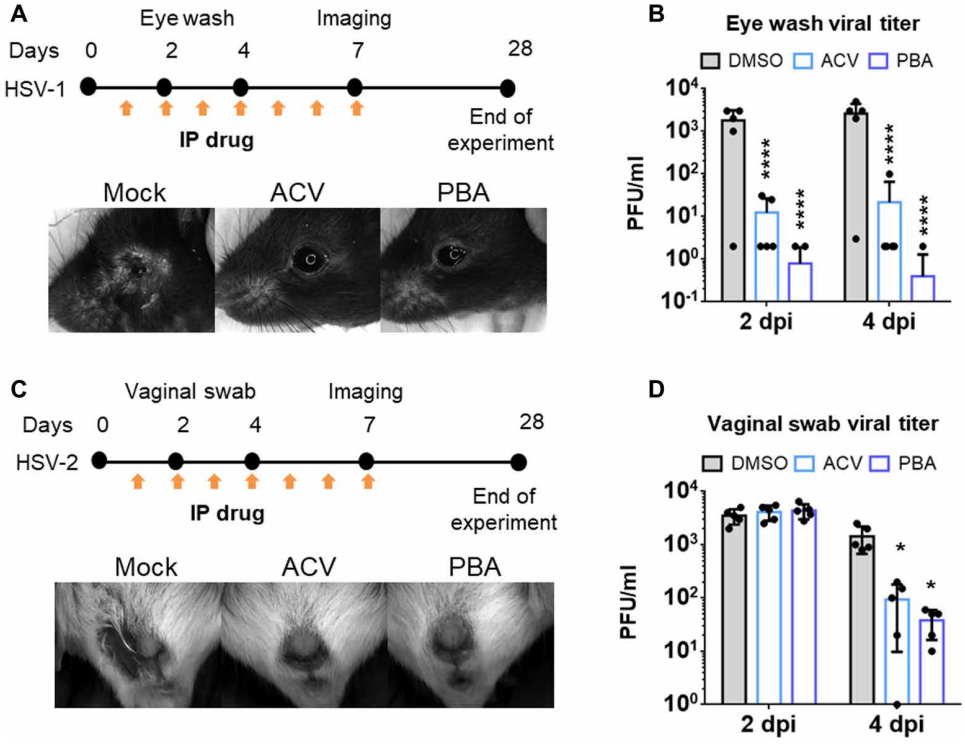

Fig. 5. Antiviral activity of PBA in murine models of ocular and genital infection. (**A**) Eight-week-old male C57BL6 mice ($n = 5$ per group) were infected with 5 × 105 PFU HSV-1 McKrae after corneal epithelial debridement with a 30-gauge needle. At 1 dpi, ACV (5 mg/kg), PBA (50 mg/kg), or PBS mock was administered to mice twice a day intraperitoneally with volume not exceeding 300 μl per dosing. Murine eyes were imaged using a Zeiss stereoscope to assess the extent of disease progression on 7 dpi. (**B**) Ocular swabs were collected on 2 and 4 dpi and used as inoculum on Vero cells to determine viral titers using a plaque assay. (**C**) The menstrual cycle of 8-week-old female BALB/c mice was synchronized using medroxy-progesterone 5 days before infecting them with 5 × 105 PFU HSV-2 333. ACV (5 mg/kg), PBA (50 mg/kg), or PBS mock was administered to mice twice a day intraperitoneally with volume not exceeding 300 μl per dosing. Infected genitalia were imaged using a Zeiss stereoscope on 7 dpi. (**D**) Vaginal swabs collected on 2, 4, and 7 dpi were used as inoculum on Vero cells to assess the viral titer using plaque assay. Two-way ANOVA was used to assess significant differences. *$P < 0.05$, ****$P < 0.0001$.

of NFκB to the nucleus. These results helped us pursue further into the possibility of using PBA as a potential therapeutic against HSV infections. While we observed antiviral ability through the systemic administration of PBA, we unexpectedly found little to no protection when PBA was administered topically. This might be due to the low bioavailability or low absorption of the drug on the corneal surface of the mouse (*32*, *33*). In addition, PBA synergized in vitro with a known topical antiviral TFT. TFT is a commonly prescribed topical antiviral to treat ocular HSV infection that needs to be dosed six to eight times every day. In mice, we have previously dosed this drug three times per day and have seen significant protection against ocular HSV infection. Hence, TFT was used as a control in our experiments (*34*). Topical drugs including TFT are required to be dosed up to 10 times every day, although novel sustained-release formulations can reduce the dosing frequency (*35*, *36*). Prolonged use of TFT has been associated with corneal toxicity including inflammation, dryness, and pain (*37*, *38*). Systemic drugs such as ACV, although very effective, can cause renal toxicity including acute kidney injury when administered intravenously (*39*, *40*). Synergizing these antiherpetic drugs with PBA can reduce the serious toxic effects associated with them. In addition, PBA showed antiviral efficacy against ACV-resistant strains of HSV-1 (fig. S14) and other herpesviruses such as bovine herpesvirus (BHV) and pseudorabies virus (PRV) (fig. S15), making it an ideal stand-alone drug candidate to treat ACV-resistant HSV infections.

PBA is a Food and Drug Administration (FDA)–approved orphan drug, marketed by Ucyclyd Pharma as Buphenyl, by Swedish Orphan International (Sweden) as Ammonaps, and by Fyrlklövern Scandinavia as triButyrate, to treat urea cycle disorders, where it helps the excretion of excess nitrogen (*41*, *42*). Given that PBA has shown the ability to cross the blood-brain barrier (*43*), the applications for its use will have greater implications in future antiviral research. Urea cycle disorder–related acute rapid-onset encephalopathy has shown to mimic HSV encephalitis (*44*) and can be misdiagnosed when using magnetic resonance imaging. Further studies might shed light into the similarities between urea cycle disorders and how HSV infection progresses into the brain.

In conclusion, this study focuses on the importance of CREB3 as a prosurvival, proviral factor that HSV uses for its own benefit. Furthermore, pharmacological mimicry of CREB3 silencing using an FDA-approved drug such as PBA can work as an excellent strategy to inhibit HSV infections. In addition, this study shows that PBA can synergistically improve the topical efficacy of TFT and systemic efficacy of ACV in restricting HSV-1–induced ocular and neuronal infections, respectively. PBA is a well-known and well-studied ER chaperone that helps alleviate ER stress by increasing protein folding capacity in the ER and effectively translocating misfolded proteins for proteosomal degradation. Synergizing with PBA could provide additional renal protection when higher amounts of antiviral drugs need to be administered systemically.

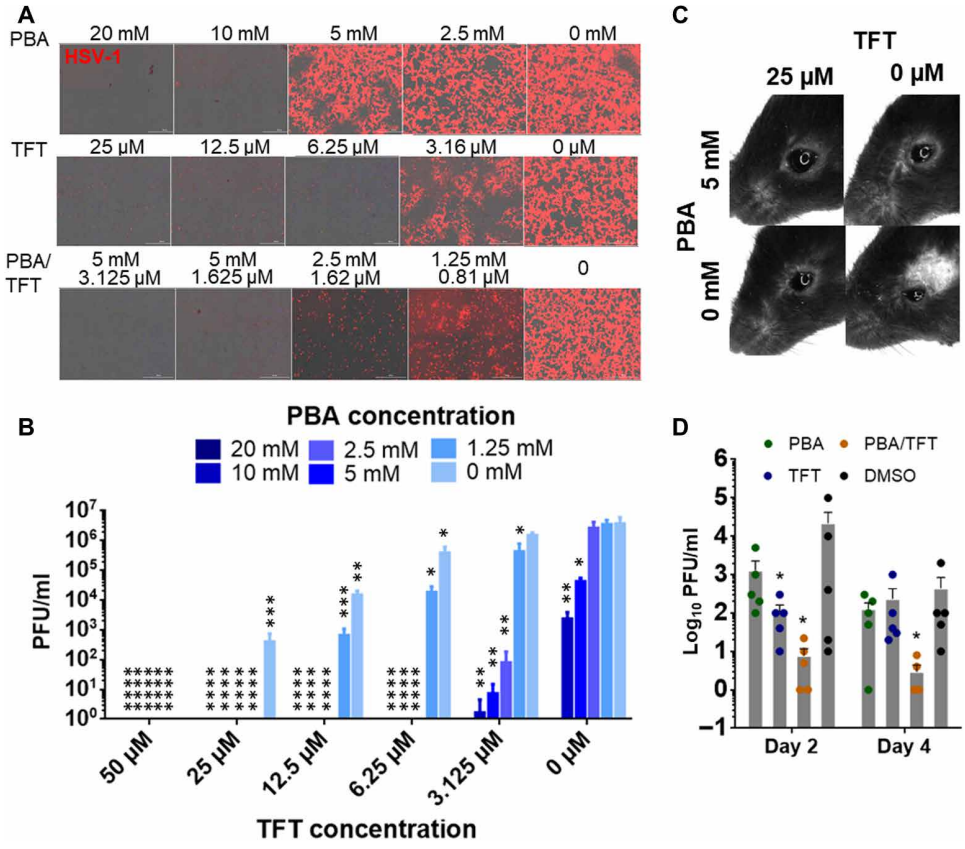

Fig. 6. PBA synergizes with ACV analogs to reduce effective antiviral concentration. HCEs infected with HSV-1 17 GFP (pseudocolored red) were treated with PBA alone, TFT alone, or PBA + TFT cocktail at shown concentrations. (**A**) The cells were imaged using a fluorescence microscope at 10× to assess the extent of viral spread. (**B**) Cell lysates were used as inoculum on Vero cells to assess the viral titer through plaque assay. PBA concentration was varied from 20 to 1.25 mM with twofold dilution per step, while TFT was used from 6.25 to 0.8 μM with twofold dilution per step. (**C**) Eight-week-old male C57BL6 mice were infected with 5×10^5 PFU HSV-1 McKrae after corneal epithelial debridement. Starting 1 dpi, murine eyes were dosed with TFT (25 μM), PBA (5 mM), PBA (5 mM) + TFT (25 μM) cocktail, or DMSO control, three times a day for 7 days. Murine eyes were imaged using a Zeiss stereoscope to assess the extent of disease progression on 7 dpi. (**D**) Ocular swabs taken 2 and 4 dpi were used as inoculum on Vero cells to assess the viral titer using plaque assay. Two-way ANOVA was used to assess significant differences. *$P < 0.05$, **$P < 0.01$, ***$P < 0.001$, ****$P < 0.0001$.

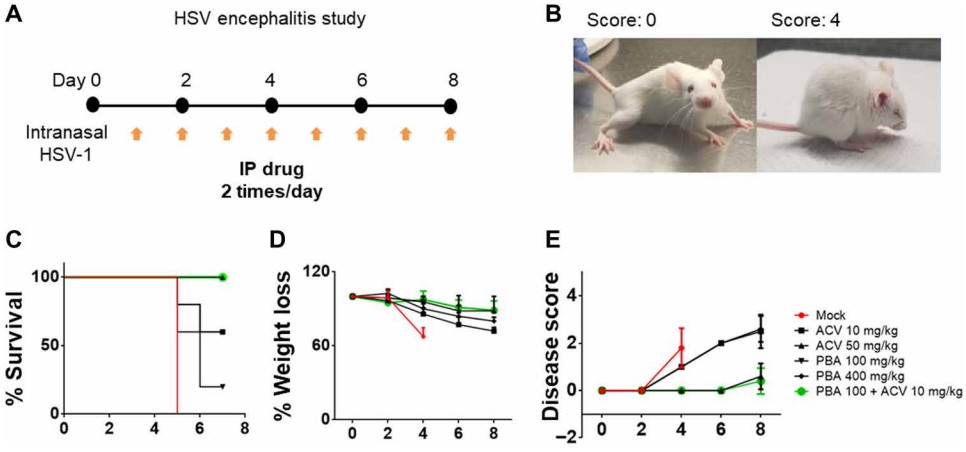

Fig. 7. PBA reduces effective ACV concentration to treat HSV encephalitis. Eight-week-old female BALB/c mice were infected with 1×10^5 PFU HSV-1 McKrae through intranasal route to induce encephalitis. (**A**) Infected mice when treated with ACV look healthier with no behavioral changes (left) compared with those left untreated (right). (**B**) Infected mice were administered ACV (50 and 10 mg/kg), PBA (100 and 400 mg/kg), or a cocktail of PBA (100 mg/kg) + ACV (10 mg/kg). (**C**) Percentage survival was calculated 10 dpi for each group based on survival criteria (no more than 20% weight loss). (**D**) Animal weights were measured daily, and animals showing acute weight loss or behavioral changes were euthanized for humane reasons. (**E**) A blinded reviewer was used to assess the disease progression and score the mice on each day.

MATERIALS AND METHODS

PBA and sodium PBA (NaPBA) were purchased and used as is from BioVisioin (1608-1000). ACV, TFT, gangiclovir, valacyclovir, famcyclovir, and pencyclovir were purchased from Selleck Chemicals, TX, USA.

Cells and viruses

HCE cells (RCB1834 HCE-T) were obtained from K. Hayashi (National Eye Institute, Bethesda, MD) and were cultured in minimum essential medium (MEM) (Life Technologies, Carlsbad, CA) with 10% fetal bovine serum (FBS) (Sigma-Aldrich, St. Louis, MO) and 1% penicillin-streptomycin (P/S) (Life Technologies, Carlsbad, CA). The human vaginal epithelial cell VK2/E6E7 was obtained from the American Type Culture Collection (VA, USA). VK2/E6E7 cells were passaged in keratinocyte serum–free medium (Gibco/BRL, Carlsbad, CA) supplemented with epidermal growth factor, bovine pituitary extract, and 1% P/S. African green monkey kidney (Vero) cells were provided by P. G. Spear (Northwestern University). Madin-Darby bovine kidney (MDBK) cells were provided by R. Longnecker's laboratory from Northwestern University. Vero and MDBK cells were passaged in Dulbecco's modified Eagle's medium (DMEM; Life Technologies, Carlsbad, CA) supplemented with 10% FBS and P/S.

HSV-1 (17 GFP, McKrae), HSV-2 (333 GFP), and β-galactosidase–expressing HSV-1 (gL86), HSV-2 (333) used in this study were provided by P. Spear's laboratory at Northwestern University. Virus stocks were propagated and titered on Vero cells and stored at −80°C. PRV and BHV were provided by G. Smith and R. Longnecker, respectively, from Northwestern University and propagated and titered on MDBK cells.

Transfection

To silence CREB3 expression, pretested siRNAs were procured from Integrated DNA Technologies as a TriFECTa RNAi Kit (Integrated DNA Technologies, USA), which consisted of three different siRNA sequences and three control sequences including a Cy3-tagged RNA to confirm transfection of the siRNA. Dilution of the siRNA molecules and transfection were performed according to the manufacturer's protocol using Lipofectamine RNAi-Max (Invitrogen, Life Technologies, Carlsbad, CA, USA) transfection reagent in Opti-MEM (Life Technologies, Carlsbad, CA) for a period of 24 hours before any further experimentation. The transfection efficiency for the siRNAs was approximately 60 to 80%. To extrinsically up-regulate CREB3, plasmid containing the CREB3-triple-FLAG tag (a.p3XFlag-LZIP) was procured from Addgene (nonprofit plasmid repository, MA, USA). Transfections were performed for 24 hours using Lipofectamine 2000 (Invitrogen, Life Technologies, Carlsbad, CA, USA) in Opti-MEM before any further experimentation. The transfection efficiency for the CREB3 plasmid was approximately 60%.

Cell viability assay

Cell viability assay using various concentrations of PBA/NaPBA was performed on HCE cells plated at a density of 1×10^4 per well in 96-well plates overnight (*45*). Concentrations starting at 100 mM were twofold serially diluted in whole media and added to cell monolayers for a period of 24 hours. At the end of incubation, 3-(4,5-dimethylthiazol-2-yl)-2,5-diphenyltetrazolium bromide (MTT; BioVision, USA) at a concentration of 0.5 mg/ml in whole media was added to cells and incubated for a period of 3 hours to allow crystal formation. Acidified isopropanol (1% glacial acetic acid v/v) was added to cells to dissolve the formazan crystals. Dissolved violet crystals were transferred to new 96-well plates and analyzed by a micropate reader (TECAN GENious Pro) at 492 nm.

Viral entry assay

β-Galactosidase–expressing viruses HSV-1 gL86 at MOI 10 was used to study viral entry into cells (*46*). HCEs were plated at a density of 1×10^4 in 96-well plates overnight before use. HSV-1 strain gL86 was mixed with multiple concentrations of PBA/NaPBA in MEM media and overlaid on HCEs to infect the cell monolayers for 6 hours, after which the cells were washed with PBS twice and 100 μl of soluble substrate *o*-nitrophenyl-β-D-galactopyranoside (ONPG; 3 mg/ml; Thermo Fisher Scientific) was added to the cells along with 0.5% NP-40 (USB Corporation, Cleveland, OH, USA) in PBS. Enzymatic activity was measured by a micropate reader (TECAN GENious Pro) at 405/600 nm.

Immunoblotting

Cells were scraped and incubated with 100 μl of radioimmunoprecipitation assay (Millipore Sigma) buffer with protease phosphatase inhibitor cocktail (Halt; Thermo Fisher Scientific) for a period of 30 min on ice. Whole-cell protein extracts (supernatant) were collected by centrifuging the mixture at 13,500 rpm on a bench top refrigerated (4°C) centrifuge for 15 min. Protein samples were then denatured in NuPAGE LDS Sample Buffer (Invitrogen, NP00007) and β-mercaptoethanol (Thermo Fisher Scientific) by heating them to 80°C for 10 min. The denatured protein samples were allowed to cool, and equal amounts of protein were added to 4 to 12% SDS–polyacrylamide gel electrophoresis loading gels and run at a constant speed of 70 V for 3 hours. The protein from the gel was then transferred to a nitrocellulose membrane (IB23001, Invitrogen) using an iBlot 2 dry transfer machine (Thermo Fisher Scientific, USA). Nitrocellulose membrane was blocked in 5% nonfat milk/bovine serum albumin (BSA) in tris-buffered saline (TBS; Thermo Fisher Scientific, USA) and 0.1% Tween 20 (Sigma-Aldrich) (TBST) for 1 hour at room temperature. After the blocking step, membranes were incubated with primary antibody at dilutions of 1:1000 overnight at 4°C. The following day, the blots were washed multiple times with TBST before the addition of horseradish peroxidase–conjugated secondary immunoglobulin G antibody (Jackson ImmunoResearch Laboratories) at dilutions of 1:10,000 at room temperature. Anti–HSV-1 gB mouse monoclonal antibody (Abcam, 6506) and anti–glyceraldehyde-3-phosphate dehydrogenase (GAPDH) (ProteinTech, 10494-1-AP) were used to evaluate extent of viral infection. All ER stress–related proteins referred to here were purchased from Cell Signaling Technology as an ER Stress Antibody Sampler Kit (CST, #9956). Luman/CREB3 antibody was purchased from ProteinTech (11275-1-AP). Primary antibodies from Cell Signaling Technology and ProteinTech were used at 1:1000 dilution, and secondary antibodies at 1:2000 dilution. Protein bands were visualized on an ImageQuant LAS 4000 imager (GE Healthcare Life Sciences) by the addition of SuperSignal West Pico maximum sensitivity substrate (Pierce, 34080). The density of the bands was quantified using ImageQuant TL image analysis software (version 7). GAPDH was measured as a loading control (*46*, *47*). Uncut Western blots used in this study are presented in fig. S16.

Cytoplasmic and nuclear extractions

The cytoplasmic and nuclear extractions were performed using a protocol previously described (*28*, *48*). Aliquots of the fractions were made and used for immunoblotting as described above.

Plaque assay

Infected cells were suspended in 500 μl of Opti-MEM before sonication using a probe sonication system at 70% amplitude for 30 s. Sonicated cell lysates or ocular/vaginal swabs were used as inoculants for a plaque assay to determine the total amount of infectious virus. In a typical experiment, Vero cells were plated at a seating density of 5×10^4 per well in 24-well plates overnight. Upon confluency, the cell monolayers were washed with PBS, and infected samples were overlaid for a period of 2 hours at multiple dilutions. The cells were then washed twice with PBS before the addition of DMEM whole media mixed with 0.5% methylcellulose (Sigma-Aldrich). The plates were incubated for 72 hours at 37°C and 5% CO_2 before they were fixed with methanol and stained with crystal violet to determine the extent of plaque formation (*46*, *49*).

HSV-1 TK12 infection and quantification

HSV-1 strain KOS-TK12 (TK12) is a recombinant virus that expresses β-galactosidase under infected cell protein 4 (ICP4) promoter and is resistant to ACV treatment. HCEs were infected with TK12 at an MOI of 0.1, followed by therapeutic treatment with either dimethyl sulfoxide (DMSO), ACV (50 μM), or PBA (10 mM) diluted in MEM. At 24 hpi, bright-field images of the infected cells were procured, and β-galactosidase substrate ONPG (3 mg/ml) was added to cells along with 0.5% NP-40 in PBS. Enzymatic activity was measured by a micropate reader (TECAN GENious Pro) at 405/600 nm (*46*).

Quantitative polymerase chain reaction assay

RNA from cells was extracted using TRIzol (Life Technologies) according to the manufacturer's described protocol. Extracted RNA was quantified using NanoDrop (Thermo Fisher Scientific, USA) and equilibrated for all samples with Molecular Biology Grade Water (Corning, USA) before they were reverse transcribed into cDNA using High-Capacity cDNA Reverse Transcription Kit (Applied Biosystems, Foster City, CA). Equal amounts of cDNA were analyzed via real-time quantitative polymerase chain reaction using Fast SYBR Green Master Mix on QuantStudio 7 Flex system (Applied Biosystems). The primers used in this study are as follows: COPB1 F (forward), AGTCCCAGAGGCGTGATTT; COPB1 R (reverse), ACATGCACGAATAGCTGGCA; Herp F, ATGGAGTCCGAGACCGAAC; Herp R, TTGGTGATCCAACAACAGCTT; CREB3L1 F, AGACCTTACAAGATGGCCGC; CREB3L1 R, CCAGATCCCTGTCGTGGAAC; CREB3L2 F, TTTGTGTCTGGAGCCGTAGC; CREB3L2 R, GGTCCACTGGGGCTTCTTTA; CREB3L3 F, GCCGGAAAATCCGGAACAAG; CREB3L3 R, GCAAGCTGACATCCGAGTCT; CREB3 F, TGGATGCTGGTGACCAAGAC; CREB3 R, GGGACAACACTCCATGCTCA (*34*).

Confocal microscopy imaging

Fluorescence confocal imaging was performed on an LSM 710 confocal microscope (Carl Zeiss) under 63× objective. Briefly, cells that were cultured and experimented in glass bottom dishes (MatTek Corporation) were washed in PBS, fixed with 4% paraformaldehyde (Electron Microscopy Sciences, Hatfield, PA) for 10 min, and then washed with PBS again. A permeabilization step was performed using 0.01% Triton X-100 (Thermo Fisher Scientific) for 10 min after fixing the cells, followed by a blocking step for 1 hour in 1% BSA (Sigma-Aldrich). Cells were then incubated with the primary antibody in 1% BSA for 1 hour. Following the washes, the cells were incubated with a secondary conjugated Alexa Flour 647 in 1% BSA for 1 hour (*49*).

Flow cytometry

Cells infected with the GFP virus were collected on 24 hpi using Hanks'-based, enzyme-free cell dissociation buffer (Gibco, 13150). Cells were washed once with PBS before they were fixed using 4% parafolmaldehyde (Electron Microscopy Sciences, USA) and suspended in fluorescence-activated cell sorting (FACS) buffer (PBS, 5% FBS). Cell suspensions were filtered through a 70-μm mesh, and resuspended in FACS buffer before analyzing them using an in-house flow cytometer (BD Accuri C6 Plus). A total of 2×10^4 cells were collected for each sample, and the analysis was performed using FlowJo (version 10) (*46*, *47*).

Infection of human corneas

Donated human corneas procured from Eversight were a donation from A. Djalilian. Human corneas (five per group; three groups) were infected with HSV-1 17 GFP virus after epithelial debridement at the center of the cornea using a 30-gauge needle. We have previously observed that depending on the length of duration between cornea isolation from the human and final use, all human corneas get differentially infected. To avoid bias, only similarly infected corneas (two per group) were chosen to conduct this experiment. At 3 dpi, GFP fluorescence from infected corneas was visualized using a Zeiss stereoscope. Starting 3 dpi, treatments including ACV (50 μM), PBA (10 mM), or DMSO control were added to the cornea media (Gibco MEM with 1% antibacterial:antifungal Gibco, and 10% FBS, Sigma US origin). The media were changed every day until 7 dpi when the extent of infection was visualized again. Ocular swabs procured on 3 and 7 dpi were quantitated for the presence of virus using a plaque assay (*50*).

Isolation of primary HCEs

Donated human corneas were gently washed, and the iris from the sclera was removed before placing them epithelium down into 1% dispase solution overnight at 4°C. The next day, using a blunt spatula, cells were dislodged from each of the corneas in PBS. Collected cells were centrifuged and resuspended in 1 ml of 0.5% trypsin for 30 s. Trypsin was neutralized with the help of 10% FBS solution in PBS, and the cells were centrifuged at 800*g* for 5 min. Collected cells were resuspended in keratinocyte media with 1% P/S and 10% FBS. The cells were then allowed to grow in a precoated flask (Gibco Coating Matrix) for 2 weeks. The first two passages of cells were discarded, and only the cells from the third passage were used for the experiments (*34*).

Human skin graft infection

Human skin grafts were purchased from Genoskin. The HypoSkin® model consists of adipose tissue for subcutaneous injection, topical, and systemic administration in a ready-to-use format. The epithelial layer of the skin was abraded using a sterilized blade, and HSV-1 17 GFP was added topically. The skin grafts were checked every day for progression of viral replication (increase in GFP fluorescence). Starting 3 dpi, either PBA (10 mM) or DMSO control was dissolved in the skin media (provided by the supplier) and added to the bottom of the Genoskin plate. This represents a systemic model of drug administration. The medicated media were changed every day, and images were procured 7 dpi. The fluorescence was quantified over the treatment period.

In vivo ocular HSV-1 infection and treatment

C57BL/6 mice ($n = 5$) bred and housed at the university biological resource laboratory (BRL) were used for ocular modeling of murine

HSV-1 infection. Standard feed and water were provided to the mice with a 12-hour light and dark cycle with no more than five mice per cage. On day 0, 6- to 8-week-old mice were anesthetized, as described previously, before the application of a topical anesthetic (proparicaine hydrochloride, 0.5%). Corneal epithelial debridement was performed using a 30-gauge needle followed by the application of 5×10^5 PFU HSV-1 (McKrae) to the eye (*46*). Intraperitoneal injections of ACV (5 mg/kg), NaPBA (50 mg/kg), or vehicle alone dispersed in 2% DMSO, 30% PEG-200 (polyethylene glycol, molecular weight 200), and 2% Tween 80 dissolved in PBS were administered starting 1 dpi. Ocular swabs, disease scores, and stereoscopic images (Carl Zeiss stereoscope) were collected on days 2, 4, 7, and 10 postinfection. At 28 dpi, the mice were euthanized, followed by cervical dissociation, and their trigeminal ganglia were incubated in DMEM whole media. Four days after incubation, the supernatants from the trigeminal ganglia suspension were titered for viral reactivation from using a plaque assay on Vero cells (*45*).

In vivo vaginal infection and treatment

Experiments involving animals were performed under a University of Illinois at Chicago-approved protocol ACC 14-091. The mice were monitored for weight loss, and disease scores were recorded in a blinded fashion for 14 days. Sick mice were euthanized according to the Institutional Animal Care and Use Committee protocol followed by the collection of ocular/vaginal tissue and lymph nodes. Ocular wash and vaginal swabs were used to assess viral titers using a plaque assay.

Ocular toxicity studies

All the ocular toxicity studies including surface dryness, optical coherence tomography, corneal sensitivity, and ocular hypertension were performed similar to methods mentioned previously by our laboratory (*45*). Drugs were administered three times every day for 4 weeks, and the readings were procured every 2 weeks.

HSV-1 encephalitis experiment

To cause encephalitis in mice, 8-week-old BALB/c mice were inoculated intranasally with 5×10^5 PFU HSV-1 (McKrae) (*26*). The procedure was performed on anesthetized mice using a sharp ultralong thin 10-μl micropipette tip in the right nostril. All the drugs requisite for this experiment were prepared in advance and stored at 4°C for later usage. ACV sodium was prepared in two different concentrations (50 and 10 mg/kg); PBA was prepared in two different concentrations (400 and 100 mg/kg); ACV + PBA cocktail was prepared in one concentration (ACV 10 mg/kg and PBA 100 mg/kg). All the drugs were formulated in such a way that requisite dosage to each mouse could be administered in 250 μl of PBS. Drugs were administered starting 1 dpi, twice a day for 10 days. Weights and disease scores were monitored every day until 10 dpi. Mice with acute weight loss (>20%) and behavioral changes were euthanized for humane reasons.

Statistical analysis

GraphPad Prism software (version 4.0) was used for statistical analysis of each group. $P < 0.05$ was considered as the significant difference among compared groups.

SUPPLEMENTARY MATERIALS

Supplementary material for this article is available at http://advances.sciencemag.org/cgi/content/full/6/49/eabd9443/DC1

REFERENCES AND NOTES

1. L. Galluzzi, A. Diotallevi, M. Magnani, Endoplasmic reticulum stress and unfolded protein response in infection by intracellular parasites. *Future Sci. OA.* **3**, FSO198 (2017).
2. A. Samali, U. FitzGerald, S. Deegan, S. Gupta, Methods for monitoring endoplasmic reticulum stress and the unfolded protein response. *Int. J. Cell Biol.* **2010**, 830307 (2010).
3. U. Woehlbier, C. Hetz, Modulating stress responses by the UPRosome: A matter of life and death. *Trends Biochem. Sci.* **36**, 329–337 (2011).
4. C. M. Oslowski, F. Urano, Measuring ER stress and the unfolded protein response using mammalian tissue culture system. *Methods Enzymol.* **490**, 71–92 (2011).
5. S. Wang, R. J. Kaufman, The impact of the unfolded protein response on human disease. *J. Cell Biol.* **197**, 857–867 (2012).
6. C. Hetz, The unfolded protein response: controlling cell fate decisions under ER stress and beyond. *Nat. Rev. Mol. Cell Biol.* **13**, 89–102 (2012).
7. P. Walter, D. Ron, The unfolded protein response: from stress pathway to homeostatic regulation. *Science* **334**, 1081–1086 (2011).
8. M. Xue, F. Fu, Y. Ma, X. Zhang, L. Li, L. Feng, P. Liu, The PERK arm of the unfolded protein response negatively regulates transmissible gastroenteritis virus replication by suppressing protein translation and promoting type I interferon production. *J. Virol.* **92**, e00431-18 (2018).
9. R. Wang, M. Moniruzzaman, E. Shuffle, R. Lourie, S. Z. Hasnain, Immune regulation of the unfolded protein response at the mucosal barrier in viral infection. *Clin. Transl. Immunol.* **7**, e1014 (2018).
10. J. H. Lin, P. Walter, T. S. B. Yen, Endoplasmic reticulum stress in disease pathogenesis. *Annu. Rev. Pathol.* **3**, 399–425 (2008).
11. D. T. Rutkowski, R. S. Hegde, Regulation of basal cellular physiology by the homeostatic unfolded protein response. *J. Cell Biol.* **189**, 783–794 (2010).
12. J. Turpin, E. Frumence, W. Harrabi, C. E. Kalamouni, P. Desprès, P. Krejbich-Trotot, W. Viranaïcken, Crosstalk between endoplasmic reticulum stress and the unfolded protein response during ZIKA virus infection. (2019).
13. A. Baer, L. Lundberg, D. Swales, N. Waybright, C. Pinkham, J. D. Dinman, J. L. Jacobs, K. Kehn-Hall, Venezuelan equine encephalitis virus induces apoptosis through the unfolded protein response activation of EGR1. *J. Virol.* **90**, 3558–3572 (2016).
14. P. Zhang, C. Su, Z. Jiang, C. Zheng, Herpes simplex virus 1 UL41 protein suppresses the IRE1/XBP1 signal pathway of the unfolded protein response via Its RNase activity. *J. Virol.* **91**, e02056-16 (2017).
15. H. F. Burnett, T. E. Audas, G. Liang, R. R. Lu, Herpes simplex virus-1 disarms the unfolded protein response in the early stages of infection. *Cell Stress Chaperones* **17**, 473–483 (2012).
16. B. P. Johnston, C. McCormick, Herpesviruses and the unfolded protein response. *Viruses* **12**, 17 (2019).
17. J. Ye, Roles of regulated intramembrane proteolysis in virus infection and antiviral immunity. *Biochim. Biophys. Acta* **1828**, 2926–2932 (2013).
18. L. Sampieri, P. Di Giusto, C. Alvarez, CREB3 transcription factors: ER-golgi stress transducers as hubs for cellular homeostasis. *Front. Cell Dev. Biol.* **7**, 123 (2019).
19. C. M. Preston, S. Efstathiou, in *Human Herpesviruses: Biology, Therapy, and Immunoprophylaxis*, A. Arvin, G. Campadelli-Fiume, E. Mocarski, P. S. Moore, B. Roizman, R. Whitley, K. Yamanishi, Eds. (Cambridge Univ. Press, Cambridge, 2007).
20. B. V. Howley, L. A. Link, S. Grelet, M. El-Sabban, P. H. Howe, A CREB3-regulated ER-Golgi trafficking signature promotes metastatic progression in breast cancer. *Oncogene* **37**, 1308–1325 (2018).
21. H. Slodzinski, L. B. Moran, G. J. Michael, B. Wang, S. Novoselov, M. E. Cheetham, R. K. B. Pearce, M. B. Graeber, Homocysteine-induced endoplasmic reticulum protein (herp) is up-regulated in parkinsonian substantia nigra and present in the core of Lewy bodies. *Clin. Neuropathol.* **28**, 333–343 (2009).
22. G. Liang, T. E. Audas, Y. Li, G. P. Cockram, J. D. Dean, A. C. Martyn, K. Kokame, R. Lu, Luman/CREB3 induces transcription of the endoplasmic reticulum (ER) stress response protein Herp through an ER stress response element. *Mol. Cell. Biol.* **26**, 7999–8010 (2006).
23. K. K. V. Haack, A. K. Mitra, I. H. Zucker, NF-κB and CREB Are required for angiotensin II type 1 receptor upregulation in neurons. *PLOS ONE* **8**, e78695 (2013).
24. H. Shimizu, S. Saito, Y. Higashiyama, F. Nishijima, T. Niwa, CREB, NF-κB, and NADPH oxidase coordinately upregulate indoxyl sulfate-induced angiotensinogen expression in proximal tubular cells. *Am. J. Physiol. Cell Physiol.* **304**, C685–C692 (2013).
25. S. J. Schachtele, S. Hu, J. R. Lokensgard, Modulation of experimental herpes encephalitis-associated neurotoxicity through sulforaphane treatment. *PLOS ONE* **7**, e36216 (2012).
26. S. J. Schachtele, S. Hu, M. R. Little, J. R. Lokensgard, Herpes simplex virus induces neural oxidative damage via microglial cell Toll-like receptor-2. *J. Neuroinflammation* **7**, 35 (2010).
27. Y. Chen, F. Brandizzi, IRE1: ER stress sensor and cell fate executor. *Trends Cell Biol.* **23**, 547–555 (2013).

28. A. M. Agelidis, S. R. Hadigal, D. Jaishankar, D. Shukla, Viral activation of heparanase drives pathogenesis of herpes simplex virus-1. *Cell Rep.* **20**, 439–450 (2017).
29. H. Xu, C. Su, A. Pearson, C. H. Mody, C. Zheng, Herpes simplex virus 1 UL24 Abrogates the DNA sensing signal pathway by inhibiting NF-κB activation. *J. Virol.* **91**, e00025-17 (2017).
30. C. Amici, A. Rossi, A. Costanzo, S. Ciafrè, B. Marinari, M. Balsamo, M. Levrero, M. G. Santoro, Herpes simplex virus disrupts NF-kappaB regulation by blocking its recruitment on the IkappaBalpha promoter and directing the factor on viral genes. *J. Biol. Chem.* **281**, 7110–7117 (2006).
31. V. Cagno, E. D. Tseligka, S. T. Jones, C. Tapparel, Heparan sulfate proteoglycans and viral attachment: True receptors or adaptation bias? *Viruses* **11**, 596 (2019).
32. I. Januleviciene, L. Siaudvytyte, R. Barsauskaite, Ophthalmic drug delivery in glaucoma—A review. *Pharmaceutics.* **4**, 243–251 (2012).
33. S. Khan, S. Warade, D. J. Singhavi, Improvement in ocular bioavailability and prolonged delivery of tobramycin sulfate following topical ophthalmic administration of drug-loaded mucoadhesive microparticles incorporated in thermosensitive in situ gel. *J. Ocul. Pharmacol. Ther.* **34**, 287–297 (2018).
34. D. Jaishankar, A. M. Yakoub, T. Yadavalli, A. Agelidis, N. Thakkar, S. Hadigal, J. Ames, D. Shukla, An off-target effect of BX795 blocks herpes simplex virus type 1 infection of the eye. *Sci. Transl. Med.* **10**, eaan5861 (2018).
35. S. Crunkhorn, Antivirals: Topical therapy for ocular herpes. *Nat. Rev. Drug Discov.* **17**, 242 (2018).
36. K. R. Wilhelmus, Antiviral treatment and other therapeutic interventions for herpes simplex virus epithelial keratitis. *Cochrane Database Syst. Rev.* **1**, CD002898 (2015).
37. R. Koganti, T. Yadavalli, D. Shukla, Current and emerging therapies for ocular herpes simplex virus type-1 infections. *Microorganisms* **7**, 429 (2019).
38. L. Koujah, R. K. Suryawanshi, D. Shukla, Pathological processes activated by herpes simplex virus-1 (HSV-1) infection in the cornea. *Cell. Mol. Life Sci.* **76**, 405–419 (2019).
39. C. Yildiz, Y. Ozsurekci, S. Gucer, A. Cengiz, R. Topaloglu, Acute kidney injury due to acyclovir. *CEN Case Rep.* **2**, 38–40 (2013).
40. R. Fleischer, M. Johnson, Acyclovir nephrotoxicity: A case report highlighting the importance of prevention, detection, and treatment of acyclovir-induced nephropathy. *Case Rep. Med.* **2010**, 602783 (2010).
41. L. Peña-Quintana, M. Llarena, D. Reyes-Suárez, L. Aldámiz-Echevarria, Profile of sodium phenylbutyrate granules for the treatment of urea-cycle disorders: patient perspectives. *Patient Prefer. Adherence* **11**, 1489–1496 (2017).
42. X. Chen, G. Zhu, L. Zhu, The antiviral effects of sodium phenylbutyrate against boHV-1 infection in vitro. *Lett. Drug. Des. Discov.* **16**, 1370–1377 (2019).
43. N.-Y. Lee, Y.-S. Kang, In vivo and in vitro evidence for brain uptake of 4-phenylbutyrate by the monocarboxylate transporter 1 (MCT1). *Pharm. Res.* **33**, 1711–1722 (2016).
44. R. A. Kadwa, N. Sankhyan, C. K. Ahuja, P. Singhi, Late-onset citrullinemia type I: A radiological mimic of herpes encephalitis. *J. Pediatr. Neurosci.* **14**, 36–37 (2019).
45. T. Yadavalli, R. Suryawanshi, M. Ali, A. Iqbal, R. Koganti, J. Ames, V. K. Aakalu, D. Shukla, Prior inhibition of AKT phosphorylation by BX795 can define a safer strategy to prevent herpes simplex virus-1 infection of the eye. *Ocul. Surf.* **18**, 221–230 (2019).
46. T. Yadavalli, J. Ames, A. Agelidis, R. Suryawanshi, D. Jaishankar, J. Hopkins, N. Thakkar, L. Koujah, D. Shukla, Drug-encapsulated carbon (DECON): A novel platform for enhanced drug delivery. *Sci. Adv.* **5**, eaax0780 (2019).
47. S. Hadigal, R. Koganti, T. Yadavalli, A. Agelidis, R. Suryawanshi, D. Shukla, Heparanase-regulated syndecan-1 shedding facilitates herpes simplex virus 1 egress. *J. Virol.* **94**, e01672-19 (2020).
48. S. R. Hadigal, A. M. Agelidis, G. A. Karasneh, T. E. Antoine, A. M. Yakoub, V. C. Ramani, A. R. Djalilian, R. D. Sanderson, D. Shukla, Heparanase is a host enzyme required for herpes simplex virus-1 release from cells. *Nat. Commun.* **6**, 6985 (2015).
49. J. Hopkins, T. Yadavalli, A. M. Agelidis, D. Shukla, Host enzymes heparanase and cathepsin L promote herpes simplex virus 2 release from cells. *J. Virol.* **92**, e01179-18 (2018).
50. N. Thakkar, D. Jaishankar, A. Agelidis, T. Yadavalli, K. Mangano, S. Patel, S. Zeynep Tekin, D. Shukla, Cultured corneas show dendritic spread and restrict herpes simplex virus infection that is not observed with cultured corneal cells. *Sci. Rep.* **7**, 42559 (2017).

Acknowledgments: We thank P. G. Spear and R. Longnecker (Northwestern University) for providing viruses and cells used in this study. We would like to thank A. Djalilian for providing the human corneas for experimentation. We thank X. Shen for the services provided in isolating primary corneal epithelial cells from human corneas. We thank V. Aakalu, M. Ali, R. Zelkha, and T. Nguyen for assisting with the ocular toxicity studies. **Funding:** This work was supported by NIH grants P30EY001792, R01EY024710, and R01AI139768 to D.S., NIH fellowship to A.A., and unrestricted funds from Research to Prevent Blindness Inc. **Author contributions:** T.Y. and D.S. designed the research. T.Y., R.S., R.K., J.H., J.A., L.K., A.I., and K.M. performed the research. T.Y., R.S., R.K., and J.A. analyzed the data. T.Y., R.K., and D.S. wrote the paper. T.Y., R.K., A.A., and D.S. edited the manuscript. **Competing interests:** D.S. and T.Y. are inventors on a provisional patent application related to this work filed by the University of Illinois at Chicago. The authors declare that they have no competing interests. **Data and materials availability:** All data needed to evaluate the conclusions in the paper are present in the paper and/or the Supplementary Materials. Additional data related to this paper may be requested from the authors.

Submitted 21 July 2020
Accepted 22 October 2020
Published 4 December 2020
10.1126/sciadv.abd9443

Citation: T. Yadavalli, R. Suryawanshi, R. Koganti, J. Hopkins, J. Ames, L. Koujah, A. Iqbal, K. Madavaraju, A. Agelidis, D. Shukla, Standalone or combinatorial phenylbutyrate therapy shows excellent antiviral activity and mimics CREB3 silencing. *Sci. Adv.* **6**, eabd9443 (2020).

Science Advances

Standalone or combinatorial phenylbutyrate therapy shows excellent antiviral activity and mimics CREB3 silencing

Tejabhiram Yadavalli, Rahul Suryawanshi, Raghuram Koganti, James Hopkins, Joshua Ames, Lulia Koujah, Aqsa Iqbal, Krishnaraju Madavaraju, Alex Agelidis and Deepak Shukla

Sci Adv **6** (49), eabd9443.
DOI: 10.1126/sciadv.abd9443